Investigating the hot gas in active brightest cluster galaxies

A.L. Ratsimbazafy[1], S.I. Loubser[1]

[1]Centre for Space Research, North-West University, Potchefstroom 2520, South Africa

E-mail: `Ando.Ratsimbazafy@nwu.ac.za`

Abstract. We investigate a crucial phase in the cooling–feedback cycle in the star forming Brightest Cluster Galaxies (BCGs) by looking at the optical emission line properties of the reheated gas that ultimately causes the cycle to repeat. We investigate the source(s) of ionisation of the gas as single dominant ionisation mechanism can reproduce the observed emission lines, and it is possible that a mixture of the heating mechanism(s) applies to the nebula(e). To identify the dominant ionisation processes, excitation sources, morphology and kinematics of the hot gas, more line ratios over the entire optical wavelength range are necessary. For this purpose, the spatially–resolved spectra over the entire optical wavelength range for eight nearby, active BCGs in X–ray luminous groups and clusters have been obtained with the Southern African Large Telescope (SALT). The sample was chosen to have Hα detections – a strong indication of star formation activity, as well as existing data from X–ray regime available. The fundamental gas properties such as electron density, gas temperature, metallicity and several abundances were derived using the spectral features across the long wavelength range. The present optical sample will be combined with the other multi–wavelength data to form a complete view of the different phases (hot and cold gas and young stars) and how they interact in the processes of star formation and feedback detected in central galaxies in cooling flow systems, as well as the influence of the surrounding intracluster medium (ICM). Here we present our preliminary results on one of those eight BCGs, Hydra A, which shows the complexity and spatial variation of the ionisation mechanisms in the nucleus.

1. Introduction

Brightest Cluster Galaxies (BCGs) are massive early-type galaxies with high luminosities, and diffuse and extended structures. They dominate the central locations in clusters. An unknown number fraction of these galaxies is very active. This challenges our point of view of most massive early–type galaxies in clusters which are believed to be "red and dead". Moreover, BCGs located at the centres of cool-core clusters show signs of activity, such as the presence of a small fraction of young stars, radio sources, emission–line nebulae, excess UV light, far–infrared emission from warm dust, and molecular hydrogen. Various star formation histories have been found in BCGs located in the centres of X–ray luminous clusters (e.g. in Ref [1]).

In the centre of the cool–core clusters, the hot intracluster gas is dense enough that it should cool quickly, leading to cooling flow that condenses and form stars. The cooling flows are in reality much smaller than predicted, as revealed by the X–ray observations. This is referred to as the "cooling flow problem". The central cluster galaxies often host radio–loud AGN which may account for the necessary heating to counteract radiative cooling. Other mechanisms have

also been proposed to explain where cooling flow nebulae obtain their energy: fast shocks, self–irradiation by the cooling hot gas, turbulent mixing layers etc. The dense core of a galaxy cluster represents a unique environment, where the hot ICM is cooling most rapidly, feedback from the AGN is most effective, and the BCG dominates the mass. This represents one of the few places in the Universe where large–scale cooling and feedback processes can be readily observed. Gas accretion models in the centres of clusters have received a lot of attention lately, e.g. the "cold–gas accretion model" which has emerged as a useful framework for interpreting various observed properties of elliptical galaxies as well as BCGs in the centres of clusters.

This project is concerned with the optical emission line properties of the reheated gas that ultimately causes the cooling–feedback cycle to repeat. The heating source(s) in BCGs currently remains uncertain as no proposed heating mechanism reproduces all the emission–line properties within the optical wavelength ranges previously observed. A single dominant mechanism may not apply to all BCG nebulae, and there may be a mixture of heating mechanisms acting within a single nebula. Thus to get more information, which will enable the dominant mechanism(s) to be identified, we measured more line ratios over the entire optical wavelength range.

2. SALT & Gemini Observations and Data reduction
Our overall sample of eight targets has been selected from the literature to have Hα detections and strong indications of star formation activity and observed with the SALT telescope. Each one of them has been analysed and modelled in detail. The SALT data were supplemented with existing long–slit data from Gemini/GMOS. The SALT data was obtained with the Robert Stobie Spectrograph (RSS) using PG0900 grating, with a 1.5" slit. However, the B600 grating was used on Gemini with two different central wavelength settings: 461 and 466 nm with a slit width of 0.75". The properties and the details of the long–slit observations with SALT and Gemini telescopes are given in Table 1 and Figure 1 for Hydra A.

The details of the SALT data reductions were given in [2]. The telluric absorption features contaminating our red spectra were not corrected. The basic Gemini data reductions, which are similar to the SALT reduction, were performed with the Gemini–specific GMOS data reduction package implemented in the standard IRAF package. The spectra were binned so that each bin in the red frame had a minimum signal–to–noise ratio (S/N) of 30. The same bins were then extracted from the blue frames to ensure identical spatial locations of the bins in the blue and red frame. This delivered a S/N ratio of minimum 20 in the blue bins. Both SALT and Gemini spectra have different pixel scales. The same spatial bins were extracted in both the SALT and Gemini data, by taking the different pixels scale into account.

The emission lines and absorption lines were fitted simultaneously by adapting the fitting code GANDALF [3]. This code accurately separates the stellar continuum and absorption lines from the ionised gas emission. First, the emission line regions were masked, and it fits the spectrum using a set of best–fitting stellar templates in the library. The emission line mask is then lifted and with the stellar kinematics fixed, it reassesses the stellar continuum by simultaneously fitting a number of Gaussian emission–line templates consisting of recombination and forbidden lines.

3. Emission line analysis
3.1. Diagnostic diagrams
Standard diagnostic diagrams (BPT) [4] rely on the line ratios I([O III]λ5007)/I(Hβ) versus I([N II]λ6584)/I(Hα), I([S II]$\lambda\lambda$6717,6731)/I(Hα) or I([O I]λ6300)/I(Hα). These diagrams can be constructed for emission line galaxies to separate ionisation from AGN and star formation. Kewley et al. [5] used a combination of photoionisation and stellar population synthesis models to place a theoretical upper limit on the location of star forming galaxies (H II regions) on the BPT diagram. Thus, the galaxies above the Kewley's criterion are defined as purely AGN. The AGN branch is generally associated with two populations of sources: the LINERs (low

α_{J2000}		09h18m05.7s
δ_{J2000}		–12d05m44s
z		0.055
E(B–V)$_{gal}$	(mag)	0.042
Exp. time with SALT	$(seconds)$	7317 R
Pixel scale with SALT	$(arcsec/pix)$	0.12
Resolution with SALT	$(\mathring{A}/pix)$	0.95
Exp. time with Gemini	$(seconds)$	3600 B
Pixel scale with Gemini	$(arcsec/pix)$	0.14
Resolution with Gemini	$(\mathring{A}/pix)$	0.91

Table 1: Hydra A properties, and the details of the long–slit observations with SALT and Gemini telescopes. The rest–frame coverage is ~5000–7500 Å for the red (R), and ~3500–5800 Å for the blue (B).
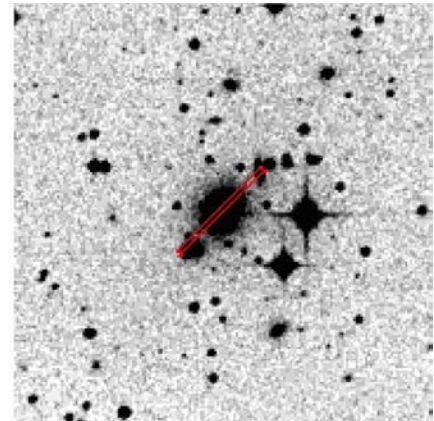
Figure 1: ESO/DSS 5 x 5 arcmin image of Hydra A with slit placement overlaid.
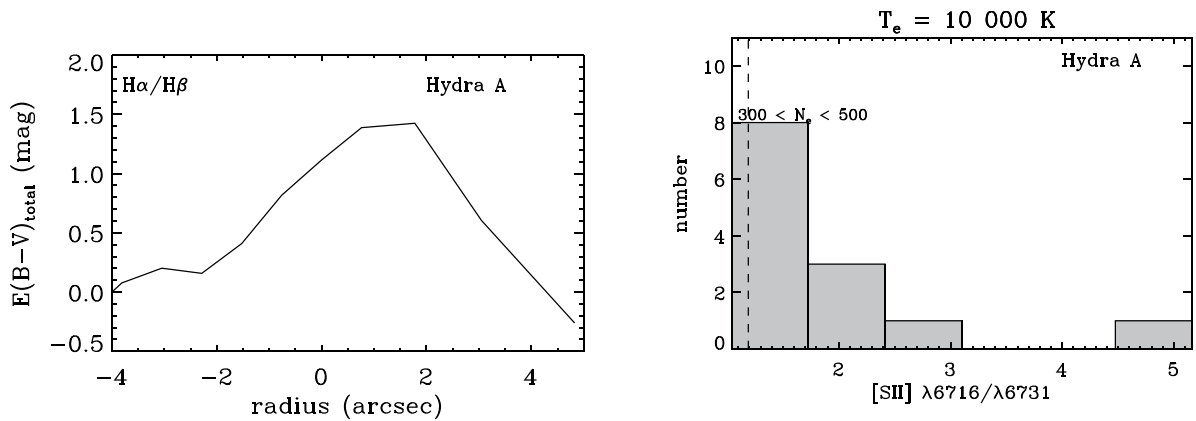
(a) The total extinction using Hα/Hβ ratio.

(b) Distribution of the line ratios for density. The total number of bins measured was 13.

Figure 2: Total extinction and electron density in Hydra A. The density of the gas in the centre of the galaxy is highlighted by the vertical dashed line.

ionisation emission) and Seyferts (high ionisation emission) regions. Kauffmann et al. [6] revised the Kewley 's criterion to a curve below which purely H II regions exist. Thus, the area between the curves contains the composite objects.

The total extinction was derived using Hα/Hβ relative strength ratios (in the red frames) and the dust extinction law given by [7] (see Figure 2a). We show three BPT diagrams for Hydra A in Figure 3. Different frames were added, taken at different conditions (notably seeing). This can account for a maximum of ~ 1 arcsec spread in the data points, nevertheless, a clear trend can be seen as the bins are located further from the nucleus of the galaxy. The centre of the galaxy shows LINER–like line ratio whereas the whole galaxy is classified as composite by looking at the [N II] diagram. It is important to note that AGN–like line ratios can also be caused by other heating mechanisms, and the ionisation regions require more detailed modelling to disentangle the complex combination of AGN feedback, photoionisation from hot stars, and other mechanisms.
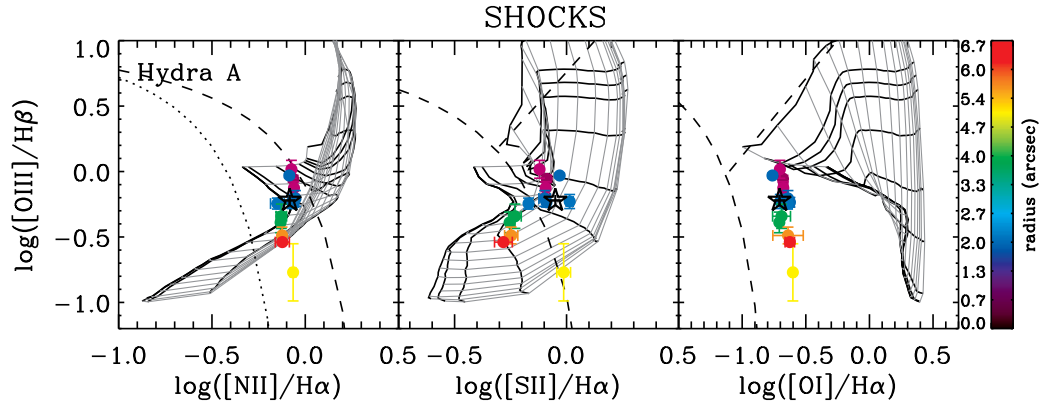
Figure 3: BPT diagrams based on [N II]λ6584/Hα (left), [S II]$\lambda\lambda$6717,6731/Hα (middle) and [O I]λ6300/Hα (right). The black star indicates the measurement across the whole galaxy (one single extracted spectrum). The demarcation by the dashed and dotted lines separates H II regions, composites and AGN as defined by [5] and [6] (see text). The model predictions for ionisation by shocks are indicated by the grids. These model predictions are from [9] with solar metallicity, pre–shock magnetic fields B from 0.001 to 100 (dark lines), and shock velocity of V from 200 to 1000 km s^{-1} (light lines – slow to fast shocks: from left to right for [S II] and [O I] diagrams, and the opposite for [N II] or precisely from top to bottom lines) and the densities n_e is 100 cm^{-3}.

3.2. Electron density and temperature

The most common means of estimating the electron density uses two emission lines of the same element which have different thresholds for collisional excitation. Doublet line ratios such as I([S II]λ6716)/I([S II]λ6731) are very useful measures of electron densities in a low–ionisation scenario. These densities, n_e, are very weakly dependent on electron temperature. The density equation are iteratively solved using a technique originally developed by [8], applied with the NEBULAR package in STSDAS, layered on the IRAF environment.

Electron temperature can similarly be measured from the I([S II]λ4068 + [S II]λ4076)/I([S II]λ6716 + [S II]λ6730) ratios (depending on the ionisation scenario), and is also very weakly dependent on electron density. We show the distribution of the [S II] line ratios for the density in Figure 2b. The line–emitting gas in nucleus (marked by the dashed line in the plot) has densities between 300 and 500 cm^{-3} (assuming T$_e \sim$ 10 000 K).

3.3. Oxygen lines and shocks

The [O III]λ4363 line can be used as an indicator for shocks. Measurements of [O III]λ4363 and He II recombination line at 4686 Å can rule out shocks as a major ionising mechanism and point toward hot stars as the primary ionising agent in the ISM. The ratio indicative of the presence/absence of shocks is given by the ratio between the [O III]λ4363 and the sum of $\lambda\lambda$4959 and 5007 lines, often called R$_{OIII}$.

Most shock models predict this ratio to be between 0.05–0.07, e.g. in Ref [10]. Photoionisation models predict smaller R$_{OIII}$ values because the [O III]–emitting gas is cooler. At a temperature of 10 000 K, R$_{OIII}$ is found to be about 0.005 in low density gas. We found that at the centre of Hydra A R$_{OIII}$ does not fall into that above limit, which strongly indicates that shocks are not the dominant ionisation process. Figure 4a illustrates the radial variation of the R$_{OIII}$ ratio.
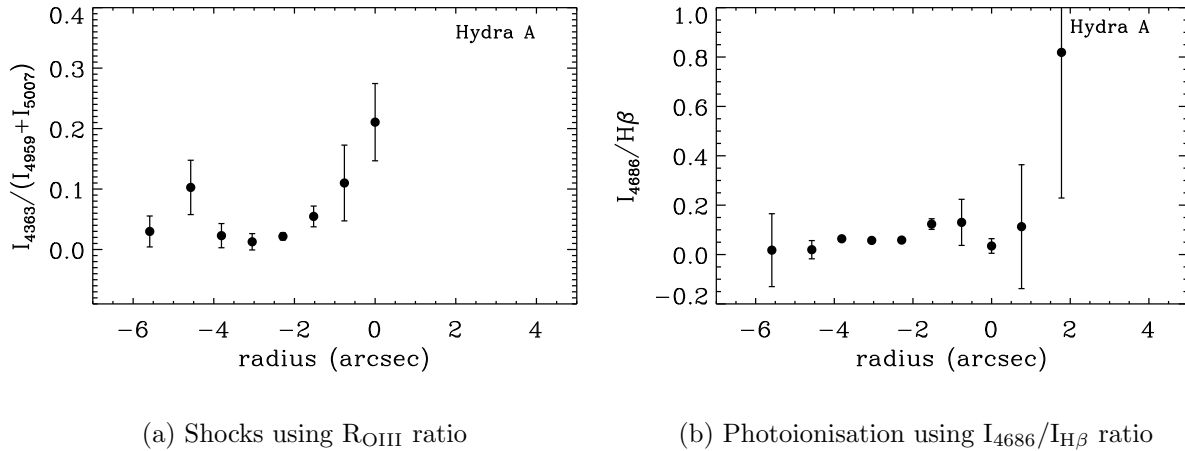
(a) Shocks using R_{OIII} ratio

(b) Photoionisation using $I_{4686}/I_{H\beta}$ ratio

Figure 4: Model independent shocks and photoionisation.

3.4. Helium recombination lines

Our blue and red spectra contain the He II recombination line at 4686 Å and He I recombination lines at 6678 Å, 5876 Å (in red spectra) and 4471 Å (in blue spectra). He I line at 6678 Å is very weak and blended by the [S II] doublet and [N II]λ6583. The most reliable measurement to be used in this case is $I_{4686}/I_{H\beta}$ in the blue spectra. The presence of a non–negligible He II recombination line for this galaxy indicates that there is harder photoionisation near the nucleus than its edge. Figure 4b demonstrates the radial variation of the He II recombination line for Hydra A.

4. Sources of ionisation

There are several possible sources of ionisation of the hot gas in the cool–cores of galaxy clusters. The most popular ideas have been: (a) the central AGN, (b) young stellar populations, (c) X–rays from the ICM, (d) heat conduction from the ICM to the cold filament, (e) shocks and turbulent mixing layers, and (f) collisional heating by cosmic rays. In Figure 3 we show our line measurements with model predictions for shocks of various speeds and magnetic field strengths from [9]. The shock models cover the same range in [N II]/Hα and [S II]/Hα data, but overpredict [O I]/Hα. These low ionisation ratios match the centre of galaxy by slow shocks ($v \sim$ 200–300 km s^{-1}) and its edge by much faster shocks ($v \sim$ 400–550 km s^{-1}).

We show other ionisation mechanisms compared to our data in Figure 5. The first panel is the model expectations for a dust–free AGN by [11], assuming a solar and a twice solar metallicities and n_e of 100 cm^{-3}. The model with a twice solar metallicity accurately predicts the [N II]/Hα ratios, but underpredicts the [S II]/Hα and [O I]/Hα ratios. However, a model with a solar metallicity is a better fit to the data. The second panel is the model prediction for collisional ionisation by cosmic rays [12]. This model produces very low [O III]/Hβ ratios. The third panel is the model expectation for the heat conduction along the boundary between the hot ICM and the cool filaments from [13]. This model fails to produce the observed ratios. Thus, cosmic rays and conduction cannot be the dominant source of ionisation in Hydra A. It is likely, however, that a combination of ionisation processes, such as shocks and AGN, are responsible for heating the gas, and is currently studied in more detail in the model independent results in sections 3.3 and 3.4.
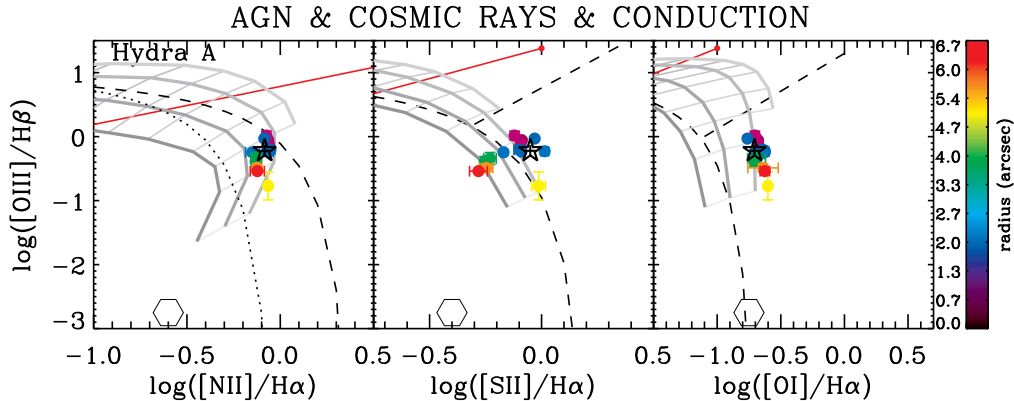
Figure 5: Similar to Figure 3, but with photoionisation by a dust–free AGN model predictions overlaid. A model with $Z = 2Z_\odot$ (in the left plot) and $Z = Z_\odot$ (in the middle and right plots), and $n_e = 100$ cm^{-3}. The grids of photoionisation are taken from [11]. From left to the right, the power–law spectral indices of $\alpha = $ –2, –1.7, –1.4 and –1.2 are indicated by the curved lines. From top to the bottom, the lines represent the ionisation parameter of $\log U = $ –4, –3.3, –2.6, –2, –1.3, –0.60 and 0. The parameter increases with [O III]$\lambda 5007$/Hβ. The conduction line (red line) is from [13] and corresponds to different initial conditions. The collisional ionisation by cosmic rays prediction is also overlaid, and indicated by a hexagon (using model predictions by [12]).

5. Conclusion

We present SALT and Gemini data for Hydra A, as part of a larger project to study eight star forming BCGs in detail, for which data has been collected mostly on SALT during a two year period. This data enables us to measure all the emission lines (with amplitude–to–noise ratio > 2) in the optical wavelength range. Our initial calculations of the hot gas properties illustrate a variety of gas kinematics and ionisation mechanisms as well as a change in hot gas properties further from the galaxy nucleus. Here, we present some preliminary results from the model independent measurements and from photoionisation models from the literature by using the BPT diagrams.

Placing the hot gas ionisation mechanisms into context with all available data from X–ray (ICM) through radio should allow for a more robust solution to this long–standing problem, while combining the hot gas kinematics with deep X–ray and radio studies may shed new light on the motions of this gas.

References

[1] Loubser S. I., et al. 2016 *MNRAS* **456** 1565
[2] Loubser S. I., Ratsimbazafy A. 2015 *in proceedings of SALT Science Conference* **PoS (SSC2015) 015**
[3] Sarzi M., et al. 2006 *MNRAS* **366** 1151
[4] Baldwin J. A., Phillips M. M., Terlevich R. 1981 *PASP* **93** 5
[5] Kewley L. J., Dopita M. A., Sutherland R. S., Heisler C. A., Trevena J. 2001 *ApJ* **556** 121
[6] Kauffmann G., et al. 2003 *MNRAS* **346** 1055
[7] Calzetti D., Armus L., Bohlin R. C., Kinney A. L., Koornneef J., Storchi-Bergmann T. 2000 *ApJ* **533** 682
[8] De Robertis M. M., Dufour R. J., Hunt R. W. 1987 *JRASC* **81** 195
[9] Allen M. G., Groves B. A., Dopita M. A., Sutherland R. S., Kewley L. J. 2008 *ApJS* **178** 20-55
[10] Dopita M. A., Sutherland R. S. 1996 *ApJS* **102** 161
[11] Groves B. A., Dopita M. A., Sutherland R. S. 2004 *ApJS* **153** 75
[12] Ferland G. J., et al. 2009 *MNRAS* **392** 1475
[13] Boehringer H., Fabian A. C. 1989 *MNRAS* **237** 1147